A bio-inspired host-parasite structure for broadband vibration energy harvesting from low-frequency random sources

Hailing Fu,[1, a)] Zahra Sharif-Khodaei,[1] and Ferri Aliabadi[1]
Structural Integrity and Health Monitoring Group, Department of Aeronautics, Imperial College London, London, SW7 2AZ, United Kingdom

(Dated: 10 April 2019)

Energy harvesting for low-power sensing has drawn great attention, but still faces challenges in harnessing broadband random motions. Inspired by the parasitic relationship in plants, a host-parasite vibration harvester is designed to scavenge random low-frequency vibrations by incorporating bi-stability and frequency up-conversion within such a design. A hosting beam is formed in a buckled condition by clamping it at both ends and applying an axial compression load. Two parasitic piezoelectric beams are fixed at the centre of the hosting beam and plucked at the free ends by two plectra on the hosting beam, while it oscillates in an inter-well mode. The low-frequency hosting beam oscillation is converted to high-frequency parasitic beam's vibration at resonance due to the plucking effect, allowing the harvester to convert broadband low-frequency motion into electricity effectively. The electromechanical dynamics are modelled, and the design was validated experimentally. The harvester is capable of harnessing low-frequency random vibration (0.0018 g^2/Hz @ 5-400 Hz) over a wide bandwidth. More than 1 mJ energy was collected over 100 s under this pseudo-random vibration.

Keywords: Vibration energy harvesting, bio-inspired energy harvester, host-parasite design, buckled beam, bi-stability, frequency up-conversion

Energy harvesting has been recognized as one of the key enablers for self-powered sensing applications in the era of the Internet of Things[1–4]. However, enhancing the energy harvesting effectiveness requires significant efforts, especially for different energy sources under various conditions, such as low-frequency human motion[5,6], random aircraft vibrations[7] or ocean waves[8]. Harnessing random, broadband and low-frequency kinetic energy is one of the key challenges, and different mechanisms have been developed to enhance the conversion performance.

Nonlinear dynamics are one major consideration to enhance the operation bandwidth[9–11]. Different harvesters have been developed using mono-stable[12–14], bistable[15–17] and multi-stable behaviors[18–20]. The aim is to alter harvesters' potential shape by applying pre-loads using magnetic forces[21–23] or displacement constraints[24,25]. A good example of a bistable harvester using displacement constraints is a device designed for harvesting energy from passing traffic and pedestrians[26]. A scissor-like structure was adopted to transfer the vertical passing weight to a horizontal axial force for buckling and excitation.

In addition to non-linearity, frequency up-conversion is another mechanism that is often employed in harvesting low-frequency motions, especially human motion[27–29]. This mechanism uses a beam plucking effect to covert the low-frequency plucking motion into high-frequency transducers' vibration, in which the transducers normally operate at resonance after each plucking. Direct impact[30] or magnetic plucking[31] are typical methods to form the plucking motion and activate the transducers. In a recent work, Halim and Park developed an impact-driven harvester for harvesting human-limb motion[32]. A metal ball was designed to impact a flexible side-wall where a piezoelectric beam is fixed. The impact motion excited the beam, and the low-frequency limb motion was up-converted to high-frequency beam vibration.

The parasitic relationship is a well-known phenomenon in nature. Fig. 1(a) provides a good example in plants, where a dodder is reliant on a host plant. In terms of motions and dynamics, the parasitic plant intertwines with the hosting plant and moves along with the host; however, due to the freedom of its own structure, the parasitic plant exhibits more complex dynamics even under simple hosting plant's motions, such as airflow-induced low-frequency vibration.

Inspired by this phenomenon, a host-parasite energy harvester incorporating bi-stability and frequency up-conversion is proposed to convert low-frequency, low-amplitude, random vibration into electricity effectively. Two parasitic piezoelectric beams (PPBs) are fixed at the center of a buckled hosting beam (BHB), as shown in Fig. 1. The BHB is fixed at both ends with the

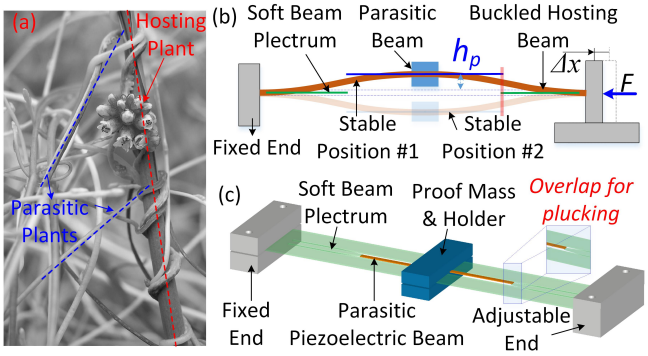

FIG. 1. (a) The host-parasite structure in plants; (b) the bio-inspired harvester schematic; (c) harvester design in 3D.

a)Electronic mail: h.fu14@imperial.ac.uk

right-side end adjustable. An axial load F is applied on the adjustable end to force the beam to be buckled with a buckled distance Δx, and two equilibrium positions are created, as shown in Fig 1(b). A proof mass is amounted at the center of the BHB to capture kinetic energy from base vibration and to reduce the BHB resonant frequency. The proof mass also serves as the holder for PPBs, as shown in Fig. 1(c).

The PPBs can be regarded as cantilever beams fixed on the proof mass of the BHB, absorbing energy from the BHB. The free ends are plucked randomly by two soft beam plectra on the BHB, when the PPBs are in contact with the plectra. Soft plectra are used to prevent the piezoelectric beam from being damaged due to the direct impact. When the proof mass operates in an inter-well mode along with the BHB, the PPBs are plucked twice per cycle by beam plectra. After plucking the PPBs vibrate freely at resonance, effectively converting low-frequency vibrations over a broad bandwidth.

The dynamics of a buckled beam with a proof mass at the centre can be described by a lumped-parameter model developed by Cottone *et al.* in Ref [33,34] or Liu *et al.* in Ref [35]. The governing equation is:

$$\frac{d^2x_b}{dt^2} + 2\xi_b\omega_0\frac{dx_b}{dt} - \frac{1}{2}\omega_0^2 x_b + \frac{1}{2}\frac{\omega_0^2}{h_p^2}x_b^3 = -\kappa_0\frac{d^2u}{dt^2} \quad (1)$$

where ξ_b is the damping ratio, x_b is the displacement of the BHB at the beam center, h_p is the buckling level, u is the base displacement, ω_0 is the linear resonant frequency for small displacement around the buckled state of h_p, and κ_0 is the inertia force factor due to the distributed mass of the buckled beam. The detailed equation and discussion about this factor can be found in the supplementary material.

The plucking motion of the PPBs are illustrated in Fig. 2. Due to the symmetrical nature of the harvester as shown in Fig. 1(b), only the left half of the harvester is illustrated. Fig. 2 shows a half-cycle motion of the BHB vibrating between two stable positions (inter-well) from Stable Position 1 to Stable Position 2. The PPB remains static before the plucking motion occurs, as shown in Fig. 2(a). When the plucking motion starts, the PPB follows the motion of the BHB and is caught by the plectrum in the central position [Fig. 2(b)]. As the BHB keeps moving downward, the PPB is released by the plectrum [Fig. 2(c)], when the proof mass displacement reaches the certain value Θ_t. Then, the PPB vibrates freely at resonance, as shown in Fig. 2(d), before the next plucking motion appears. The PPB displacement regarding to the BHB proof mass during the whole process is illustrated in Fig. 2(e). Based on the above analysis, the PPBs' displacement x_p can be expressed as

$$x_p = \begin{cases} x_b, & \text{during plucking}, \mid x_p \mid < \Theta_t, \\ x_p, & \text{after plucking} \mid x_p \mid \geq \Theta_t. \end{cases} \quad (2)$$

It is worth mentioning that the impact dynamics between the PPBs and plectra are not modelled; the plucking effect is simply modelled as a resultant PPB displacement due to plucking, as show in Eq. (2).

The dynamics of the PPBs after each plucking, namely the free vibration shown in Fig. 2(d), can be calculated using the theory developed by Erturk and Inman in Ref. [36]. The plucking effect is considered as the initial condition for the PPB's free vibration. The electromechanical dynamics of the PPBs can be expressed as

$$\frac{d^2\eta_r(t)}{dt^2} + 2\zeta_r\omega_r\frac{d\eta_r(t)}{dt} + \omega_r^2\eta_r(t) - \vartheta_r V(t) = -m\frac{d^2x_b}{dt^2}\int_0^{L_p}\phi_r(x)d(x), \quad (3)$$

where $\phi_r(x)$ and $\eta_r(t)$ are the mass normalized eigenfunction and the modal mechanical coordinate of the cantilever beam with respect to its rth modal shape, ζ_r is the modal damping ratio, ω_r is the effective undamped modal frequency, ϑ_r is the piezoelectric coupling term in physical coordinates, $V(t)$ is the voltage on the PPB, and m is the mass per unit length of the PPB.

As a piezoelectric beam is equivalent to a capacitor in parallel to a current source[36], another governing equation can be obtained, as

$$C_p\frac{dV(t)}{dt} + \frac{V(t)}{R_l} + \sum_{r=1}^{\infty}\vartheta_r\frac{d\eta_r(t)}{dt} = 0, \quad (4)$$

where C_p is the inherent capacitance of the PPB and R_l is the resistive load connected to the PPB. The tip displacement x_p of the PPB can be obtained using

$$x_p(L_p, t) = \sum_{r=1}^{\infty}\phi_r(L_p)\eta_r(t). \quad (5)$$

These equations can be numerically solved in Matlab/Simulink, and the dynamics for both the BHB and PPB can be obtained. The numerical results will be shown and discussed with experimental results.

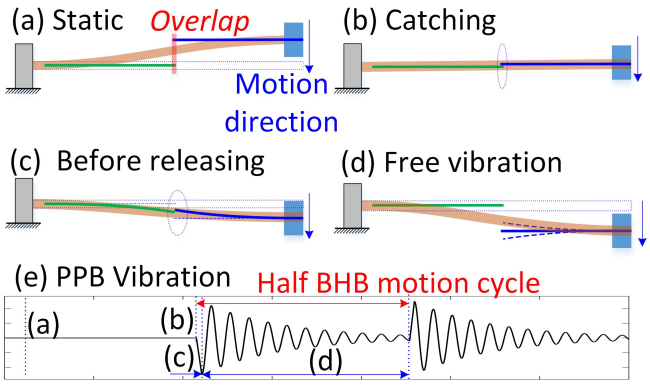

FIG. 2. Plucking illustration. Due to the symmetrical nature of the harvester, only left half of the harvester is illustrated. (a) Static position of the harvester; (b) the PPB is caught by the plectrum, and plucking motion starts; (c) the terminating position of the plucking motion; (d) the PPB is released and vibrate freely at resonance; (e) the PPB displacement in the whole process with the position of (a) - (d) marked.

A prototype was fabricated and tested under different vibration conditions. The prototype and experimental set-up are shown in Fig. 3. A high-density polythene film ordered from RS Components was laser-cut for the BHB. The low stiffness of this material is ideal for the BHB to be buckled and operate in the inter-well mode from low-acceleration vibrations. Beam plectra were laser-machined from the BHB in a form of cantilever beams, as shown in Fig. 3(a). These soft plectra are critical to protect the piezoelectric beam from being damaged by the direct impact.

A proof mass printed by a 3D printer CONNEX 350 using the material Verowhite Plus is fixed in the middle of the BHB, as shown in Fig. 3(a). The proof mass is designed to capture energy from base vibration and also to decrease the harvester's optimal operation frequency. This reduced frequency is ideal for harvesting low-frequency vibrations. Meanwhile, the proof mass also serves as the holder for PPBs, as shown in Fig. 3(a) and (b). Two PPBs ordered from Johnson Matthey Piezo Products with the material model number of M1100 are clamped on and carried by the proof mass. The dimensions are 26.5 × 1.5 × 0.3 mm. The design parameters and material proprieties are summarized in Table S1 in the supplementary material.

The harvester was mounted on a fixture, as shown in Fig. 3(b). The BHB is clamped at both ends with one adjustable end. The buckling level can be adjusted by pre-setting the horizontal position of the adjustable end. Eventually, the whole assembly was mounted on a shaker, as shown in Fig. 3(c), and tested under different vibration conditions. The beam displacement was measured using a laser sensor from Keyence (LK-G5001P).

In order to examine the bistale and frequency up-converting dynamics, the BHB was set at a high buckling level (h_p = 2.5 mm), and plucked manually on the proof mass using a plectrum at a low frequency. The system dynamics are illustrated in Fig. 4. The displacement was measured at the tip of the PPB regarding to the ground. In each plucking moment, the BHB jumps from one stable position to another, during which the PPB is plucked, and after being plucked, the PPB oscillates freely at resonance (376 Hz). Electricity is converted from the vibration of the PPB. The plucking moments for different stable positions are illustrated in Fig. 4(III) and (IV), and the resultant output voltage of the corresponding plucking is shown in Fig. 4(I) and (II).

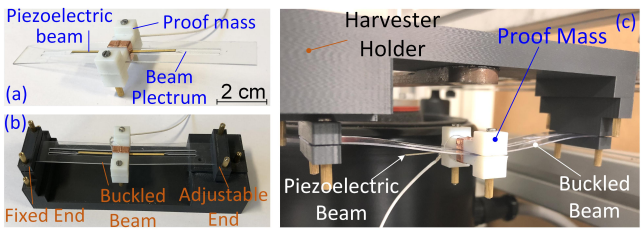

FIG. 3. Prototype and experimental set-up. (a) Assembly of the broadband energy harvester; (b) harvester mounted on a fixture with one adjustable end for buckling; (c) testing set-up with the harvester fixed on a shaker.

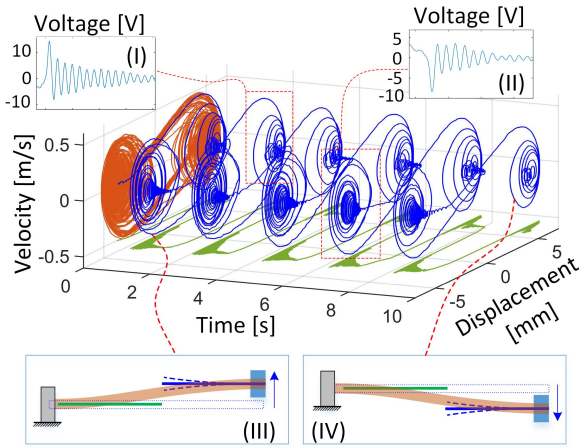

FIG. 4. Measured PPB displacement and velocity in time, illustrating the bi-stability of the BHB and the frequency up-converting dynamics of the PPB. (I) and (II) PPB output voltage after plucking; (III) and (IV) two different plucking situation in one BHB motion cycle.

The system dynamics in the frequency domain was examined through frequency sweeping tests, as shown in Fig. 5. A constant acceleration 0.82g was applied on the harvester; Fig. 5(a) and (b) are the base displacement for the frequency forward and backward sweeping tests respectively. The vibration dynamics of the BHB are shown in Fig. 5(c)(forward) and (d)(backward). A broad bandwidth is exhibited, namely 22 - 32 Hz for forward sweep and 15 - 22 Hz for backward sweeping, in which the BHB vibrates in the inter-well mode. The PPB can be plucked twice in each cycle. The PPB displacement is illustrated in Fig. 5(e) and (f). Although the BHB may not vibrate in the inter-well mode, the PPB can also be impacted by the plectra in a collision but non-plucking manner. This effect also indicates in the PPB displacement curve, such as the spikes between 11 - 13 Hz and the vibration between 22 - 27 Hz in the backward sweep curve in Fig. 5(f). The motion from 11 to 13 Hz are caused by the sub-harmonic resonances in bistable structures[37].

The output voltage from the PPB is shown in Fig. 5(g)

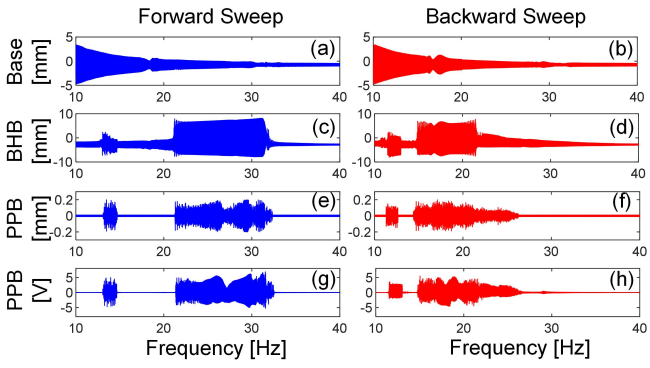

FIG. 5. Measured forward and backward sweeping performance. (a) and (b) base excitation displacement (0.82g); (c) and (d) BHB displacement; (e) and (f) PPB displacement; (g) and (h) PPB output voltage measured on a 94 kΩ resistor.

and (h). The bandwidth follows the same trend as the PPB displacement. It is worth mentioning that the output voltage fluctuates for different excitation frequencies. This fluctuation can be explained using the dynamics shown in Fig. 4. When the excitation frequency is high, the short BHB plucking period does not allow the PPB to be fully damped down after each plucking. The oscillating PPB can interfere with the forthcoming plucking motion from the BHB, resulting in the variation of the beam dynamics.

In order to further investigate the bistable and plucking dynamics, the velocity-displacement phase portrait was investigated theoretically and experimentally, as shown in Fig. 6. The displacement discussed here is the PPB tip displacement regarding to the shaker. Two plucking moments in each BHB motion cycle can be identified (dash line). The portrait fluctuation after each plucking is due to the PPB oscillation. The dynamics for different excitation frequencies are illustrated, showing the dynamics for different vibration conditions. The discrepancy between the theoretical and experimental results can be from the neglect of the impact dynamics between the PPBs and plectra, the asymmetric potential shape of the BHB due to gravity or the difference in boundary conditions.

The system performance under different excitation levels are illustrated in Fig. 7 for the forward and backward sweeping tests, respectively. As indicated, the bandwidth of the harvester increases with the increase of acceleration

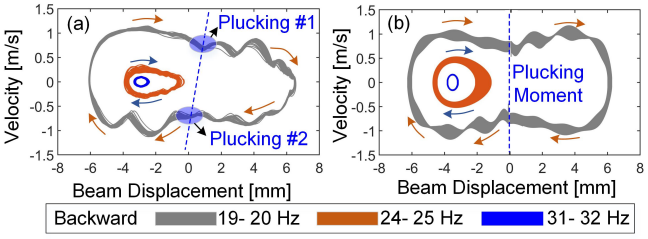

FIG. 6. Measured and simulated displacement-velocity phase portrait for different operation frequencies. (a) Measured and (b) simulated results for the backward sweeping dynamics.

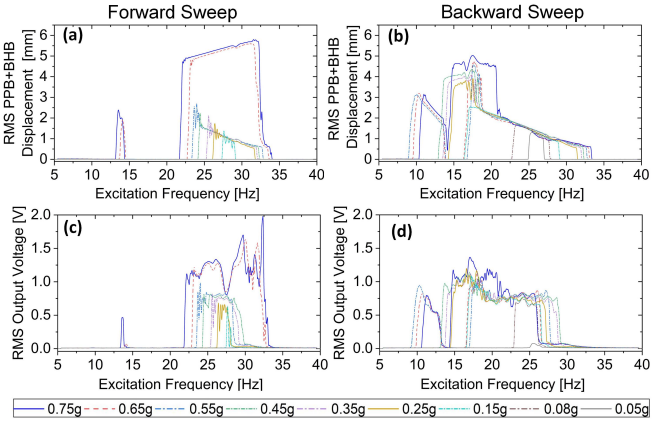

FIG. 7. PPB displacement and voltage frequency sweeping performance for different acceleration levels. Forward sweeping for the left column and backward sweeping for the right.

levels. The inter-well oscillation is ideal for the system to convert more energy into electricity. However, when the BHB oscillates in the intra-well mode, the system can still generate certain amount of energy over a bandwidth, such as the output voltage at 0.25g. This is due to the impact between the PPB and the plectra, when they are in contact, as shown Fig. 2(b). In this case, the BHB motion is not strong enough to carry the PPB to the second stable position, but the PPB can still be in contact with the plectra. This collision further extends the harvester frequency bandwidth.

In practice, vibrations can be random and broadband. In order to examine the performance, a pseudo-random vibration test was conducted, and the results are illustrated in Fig. 8. The vibration bandwidth is from 5 to 400 Hz with a power spectral density of 0.0018 g^2/Hz, as shown in Fig. 8(a). The output voltage and generated energy are depicted in Fig. 8(b). More than 1 mJ energy was generated within 100 s. The detailed dynamics are illustrated in Fig. 8(c), showing the frequency up-converting behaviour under low-frequency, random base excitation.

In order to evaluate the performance of the harvester developed in this work, a comparison with the harvesters in the literature is provided in Table I. The harvester from Huguet *et al.*[17] exhibits a wide operation bandwidth (80 Hz), but the central frequency is relatively high (120 Hz). The normalized power density is quite low compared to others. The work from Yi *et al.*[22] has the highest power density (150 mW/cm^3), but this value was obtained with a relatively high acceleration level and with a high central frequency and narrow bandwidth. In comparison, the work in this paper exhibits enhanced performance in operating bandwidth (18 Hz centred at 23 Hz) at low frequency and improved normalized power density (1.338 mW/cm^3/g^2/Hz) at low-amplitude excitation (0.25 g), further illustrating the advantages in har-

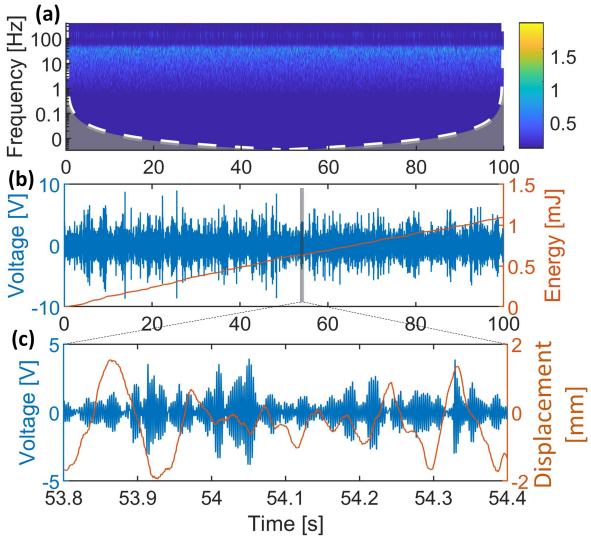

FIG. 8. System performance under pseudo-random excitation (5 - 400 Hz; 0.0018 g^2/Hz). (a) Frequency distribution of the input excitation in time; (b) voltage and generated energy; (c) detailed voltage and base displacement between 53.8 - 54.4 s.

TABLE I. Performance comparison of broadband piezoelectric energy harvester in the literature.

Reference	Operation Mechanism	Piezo Material Volumn [mm^3][a]	Accel. [g]	Bandwidth 3-dB [Hz]	Central Frequency	Power [uW]	Power Density [mW/cm^3]	Normalized Density [mW/cm^3/g^2/Hz]
Jung & Yun[11]	Buckling Up-Converting	8×4×0.052	3	22	30	2.9	1.74	0.006
Kumar *et al.*[14]	Monostable Magnetic	28×7×0.3	N/A	N/A	N/A	16.8	0.29	N/A
Gafforelli *et al.*[25]	Buckling	76.2×14×0.3	0.5	8	64	98	0.31	0.018
Huguet *et al.*[17]	Bistable & Subharmonic	28×10×0.1	0.51	80	120	269	9.6	0.231
Yi *et al.*[22]	Bi-stability	16×5×0.05	2	15	105.3	600	150	0.356
Nguyen *et al.*[23]	Buckling	70×10×0.05	0.7	7	11	4	0.11	0.016
This work	Buckling	26.5×1.5×0.2	0.25	18	23	10.6	1.34	1.338
	Plucking		0.08	4	24.5	5.2	0.66	4.182 [b]

[a] Only the dimensions of the piezoelectric materials are considered here; the total dimensions need to be considered in actual design.
[b] The results for this work were calculated using the data for the backward sweep test in Fig. 7(d).

vesting low-frequency, low-amplitude vibration.

In summary, a bio-inspired host-parasite harvester is proposed, modelled and experimentally tested for harnessing low-frequency random vibrations. Two PPBs were mounted on and plucked by a BHB, while oscillating in the inter-well mode. The system dynamics were investigated for different excitation frequencies, acceleration levels and random-vibration conditions, showing the capability of the harvester in harnessing low-frequency, low-acceleration random vibrations over a wide bandwidth. More than 1 mJ energy was generated within 100 s under a low-amplitude pseudo-random vibration condition (0.0018 g^2/Hz @ 5 - 400 Hz).

SUPPLEMENTARY MATERIAL

See supplementary material for the discussion of possible harvester configurations, calculation of the inertia force factor and the harvester design parameters.

[1] P. D. Mitcheson, E. M. Yeatman, G. K. Rao, A. S. Holmes, and T. C. Green, Proceedings of the IEEE **96**, 1457 (2008).
[2] H. Liu, J. Zhong, C. Lee, S.-W. Lee, and L. Lin, Applied Physics Reviews **5**, 041306 (2018).
[3] H. Fu, Z. S. Khodaei, and M. F. Aliabadi, IEEE Internet of Things Journal (2018).
[4] W. Liu, A. Badel, F. Formosa, Q. Zhu, C. Zhao, and G.-D. Hu, IEEE Transactions on Industrial Electronics **65**, 3899 (2018).
[5] J. Cao, W. Wang, S. Zhou, D. J. Inman, and J. Lin, Applied Physics Letters **107**, 143904 (2015).
[6] H. Liu, C. Hou, J. Lin, Y. Li, Q. Shi, T. Chen, L. Sun, and C. Lee, Applied Physics Letters **113**, 203901 (2018).
[7] M. Q. Le, J.-F. Capsal, M. Lallart, Y. Hebrard, A. Van Der Ham, N. Reffe, L. Geynet, and P.-J. Cottinet, Progress in Aerospace Sciences **79**, 147 (2015).
[8] L. Xu, T. Jiang, P. Lin, J. J. Shao, C. He, W. Zhong, X. Y. Chen, and Z. L. Wang, ACS nano **12**, 1849 (2018).
[9] R. Harne and K. Wang, Smart materials and structures **22**, 023001 (2013).
[10] A. Hajati and S.-G. Kim, Applied Physics Letters **99**, 083105 (2011).
[11] S.-M. Jung and K.-S. Yun, Applied Physics Letters **96**, 111906 (2010).
[12] W. Wang, J. Cao, D. Mallick, S. Roy, and J. Lin, Mechanical Systems and Signal Processing **108**, 252 (2018).
[13] S. Zhou, J. Cao, and J. Lin, Nonlinear Dynamics **86**, 1599 (2016).
[14] A. Kumar, S. F. Ali, and A. Arockiarajan, Applied Physics Letters **112**, 233901 (2018).
[15] S. C. Stanton, C. C. McGehee, and B. P. Mann, Physica D: Nonlinear Phenomena **239**, 640 (2010).
[16] H. Fu and E. M. Yeatman, Mechanical Systems and Signal Processing (2018), https://doi.org/10.1016/j.ymssp.2018.04.043.
[17] T. Huguet, A. Badel, and M. Lallart, Applied Physics Letters **111**, 173905 (2017).
[18] J. Cao, S. Zhou, W. Wang, and J. Lin, Applied Physics Letters **106**, 173903 (2015).
[19] D. Younesian and M.-R. Alam, Applied Energy **197**, 292 (2017).
[20] S. Zhou and L. Zuo, Communications in Nonlinear Science and Numerical Simulation **61**, 271 (2018).
[21] L. Haitao, Q. Weiyang, L. Chunbo, D. Wangzheng, and Z. Zhiyong, Smart Materials and Structures **25**, 015001 (2015).
[22] Z. Yi, Y. Hu, B. Ji, J. Liu, and B. Yang, Applied Physics Letters **113**, 183901 (2018).
[23] M. S. Nguyen, Y.-J. Yoon, O. Kwon, and P. Kim, Applied Physics Letters **111**, 253905 (2017).
[24] J. Zhang, J. Zhang, C. Shu, and Z. Fang, Applied Physics Letters **110**, 183903 (2017).
[25] G. Gafforelli, A. Corigliano, R. Xu, and S.-G. Kim, Applied Physics Letters **105**, 203901 (2014).
[26] M. Ansari and M. A. Karami, Smart Materials and Structures **24**, 115005 (2015).
[27] W. Wang, J. Cao, C. R. Bowen, D. J. Inman, and J. Lin, Applied Physics Letters **112**, 213903 (2018).
[28] P. Pillatsch, E. M. Yeatman, and A. S. Holmes, Sensors and Actuators A: Physical **206**, 178 (2014).
[29] Y. Shu, W. Wang, and Y. Chang, Smart Materials and Structures **27**, 125006 (2018).
[30] L. Gu and C. Livermore, Smart Materials and Structures **20**, 045004 (2011).
[31] H. Fu and E. M. Yeatman, Energy **125**, 152 (2017).
[32] M. A. Halim and J. Y. Park, Microsystem Technologies **24**, 2099 (2018).
[33] F. Cottone, L. Gammaitoni, H. Vocca, M. Ferrari, and V. Ferrari, Smart materials and structures **21**, 035021 (2012).
[34] F. Cottone, M. Mattarelli, H. Vocca, and L. Gammaitoni, The European Physical Journal Special Topics **224**, 2855 (2015).
[35] W. Liu, F. Formosa, A. Badel, and G. Hu, Journal of Sound and Vibration **409**, 165 (2017).
[36] A. Erturk and D. J. Inman, Smart materials and structures **18**, 025009 (2009).
[37] J. Yang, M. A. Sanjuán, and H. Liu, Communications in Nonlinear Science and Numerical Simulation **30**, 362 (2016).